Vapour-mediated sensing and motility in two-component droplets

Nate J. Cira, Adrien Benusiglio, Manu Prakash

Title: Vapour mediated sensing and motility in two-component droplets

Authors: N. J. Cira[1], A. Benusiglio[1] & M. Prakash[1*]

Affiliations:

[1] Department of Bioengineering, Stanford University, CA

* Correspondence to: manup@stanford.edu

Summary Paragraph

When droplets of food colouring (containing propylene glycol (PG)) are mixed with water and placed on a clean glass slide, they spontaneously move in beautiful and intricate patterns (Fig. 1a, Supplemental Video 1). This perplexing observation hinges on the interplay between two key aspects of droplets: wetting and motion. Liquid wetting can range from complete as in the tears of wine effect[1,2], to minimal on a lotus leaf[3] and plays a role in industrial applications such as water-repellent coatings[4] and lubrication[5]. Controlling droplet movement is important in microfluidic liquid handling[6], on self-cleaning surfaces[7], and in heat transfer[8]. Droplet motion can be achieved by gradients of surface energy caused by chemical[9], optochemical[10], electrochemical[11], thermal[12] and mechanical[13] means. However, these techniques require either a large gradient or a carefully prepared surface[9] to overcome the effects of contact line pinning which usually limit droplet motion[14]. Here we show that two-component droplets of well-chosen miscible liquids such as PG and water deposited on clean glass are not subject to pinning and cause the motion of neighbouring droplets over a distance. Unlike the canonical predictions for these liquids on a high-energy surface, these droplets do not spread completely but exhibit an apparent contact angle. We demonstrate experimentally and analytically that these droplets are stabilized by evaporation induced surface tension gradients and that they move in response to the vapour emitted by neighbouring droplets. Our fundamental understanding of this system enabled us to construct a wide variety of autonomous fluidic machines out of everyday materials. We expect this easily reproducible system will be useful in studying multi-body interactions[15], minimal systems of sensing and actuation, and as a physical analogue for the migration of keratocytes[16] and chemotaxing cells[17].

Text:

We observed that pure water and pure propylene glycol (PG) spread completely when placed on corona treated clean glass slides (Supplementary Information section 1). This is expected on such a high energy surface for which the spreading parameter, defined as $S = \gamma_{SV} - (\gamma_{LV} + \gamma_{SL})$, is larger than zero, where γ represents the surface energy of the solid/vapor, liquid/vapor, and solid/liquid interfaces[18]. Surprisingly, mixtures of PG and water formed droplets with apparent contact angles, θ_{app}, even though $S \geq 0$. The trend in θ_{app} went from zero to a maximum value and back to zero as PG was added to water (Fig. 2a) which cannot be simply explained by the monotonically decreasing liquid/vapour surface tension (Extended Data Fig. 1)[19]. Breathing on a

droplet noticeably modified the contact angle. To quantify this observation, we deposited droplets in controlled humidity chambers and found that apparent contact angle decreased with relative humidity, and droplets spread under saturated humidity (Fig. 2b), suggesting vapour played a role in droplet stabilization.

Using tracer beads (1 µm diameter) we visualized an internal flow from centre to edge along the bottom of the droplet, similar to the flow in the 'coffee ring' effect[20]. We also observed a flow from the edge to the centre along the top of the droplet, at higher velocity than the outward flow (Fig. 2d and 2e). This less commonly seen 'counter flow' has been observed with surfactant or thermal gradients only in pinned droplets[21,22]. It collects tracer beads at the liquid-vapour interface into a prominent ring (Fig. 2e). Microscopic observation of the droplets revealed a thin film extending tens of micrometres from the edge of the bulk droplet into which the 1 µm tracer beads did not enter (Fig. 2d, Supplementary Video 4). For the same droplets on a lower energy surface the counter flow was confined to the border of the droplet (Fig. 2d). No tracer bead ring appeared (Supplementary Video 4). There was no thin film around the droplets, and the droplets were less mobile and did not interact.

From these observations we can understand the mechanism which prevents complete spreading. The high energy surface favours spreading of the droplet, as seen for pure liquids[23]. For a two-component droplet, the more volatile compound (water here) evaporates more quickly than the less volatile compound (PG). Evaporation is faster at the border of the droplet than the bulk[20], and the border of the droplet has a higher surface area to volume ratio. Therefore PG, with a lower γ_{LV} than water, is left in higher concentration at the border than the bulk. The resulting gradient of surface tension pulls liquid towards the centre along the top of the droplet, an effect shown to slow down or stop spreading[5,24,25]. Here the spreading is stopped resulting in a droplet with a stable apparent contact angle (Extended Data Fig. 2) surrounded by a thin film(Fig. 2d, 3a).[5]

Next we build a simple model to test this mechanism of droplet stabilization. We assume a sharp transition of surface tension between the bulk droplet (γ_{LVdrop}) and the surrounding thin film (γ_{LVfilm}). We introduce a quasi-static horizontal force balance at the intersection of the thin film and the bulk droplet, $\gamma_{LVdrop}\cos(\theta_{app}) = \gamma_{LVfilm}$. To calculate θ_{app}, we model the water loss from the thin film due to evaporation, estimating the water fraction and surface tension of the film as a function of external relative humidity (RH) and water fraction of the droplet (Supplementary Information section 2.3, Extended Data Fig. 3 and 4). Using this model we fit a single parameter for 40% RH and observe that the prediction globally captures the non-monotonic contact angle curve and accounts for variation in this curve as a function of relative humidity (Fig. 2a). Our current model only accounts for water evaporation, and is therefore less accurate at high PG concentration and high humidity.

Based on this model, for any two miscible chemicals on a high-energy substrate, droplets should form if and only if one of the chemicals in the mixture has both a higher surface tension and higher vapour pressure (quadrant I and III, Fig. 2c). To test this law, we placed various two-component mixtures on corona treated slides. In about 200 unique combinations (Extended Data Table 1), droplet formation vs spreading was well predicted, excluding reactive pairs (Fig. 2c), and these droplets had similar attributes to the PG/water system, such as high mobility and interactions. We also deposited PG/water droplets on other high-energy substrates - piranha treated glass, clean silicon wafers, and freshly scraped steel - and found similar behaviour.

These two-component droplets have characteristics of both wetting and non-wetting liquids: they maintain a defined contact angle, but sit on a thin fluid film. As long as $S \geq 0$, the droplets should not 'feel' the solid surface, and chemical inhomogeneities and roughness should not cause pinning. The droplet contact angle is also independent of the substrate (γ_{SV}) and surface roughness. Without pinning, the droplets display high mobility and hence move under the influence of minute forces. We do not observe high mobility on low energy surfaces with a three phase contact line, where high hysteresis inhibits droplet motion.

When two droplets were deposited at distances of up to several radii apart, they moved toward each other from over a wide range of concentrations, even when both droplets had the same concentration (Fig. 1b, 1c, 3c). Droplets increased speed as they approached each other (Fig. 3b). These long-range interactions were preserved even across a break in the glass slide (Supplementary Video 5). PG/water droplets followed a pipette tip containing water placed near but not touching the droplet or the glass slide (Supplementary Video 6). These observations and our measurements of θ_{app} vs RH (Fig. 2b) led us to the surprising conclusion that long-range interactions were vapour mediated.

Based on the observations above, we propose a mechanism for vapour-mediated interactions different than in previous systems[26,27]. Evaporation from a sessile droplet is known to produce a vapour gradient[28]. Since the vapour pressure of water is 100 times larger than the vapour pressure of PG, the dominant vapour is water. Two neighbouring droplets each lie in a gradient of water vapour produced by the other (Fig. 3a). This gradient causes a local increase in relative humidity and thus decreased evaporation of the thin film on the adjacent portions of the droplets, breaking symmetry. The decreased evaporation leads to an increased water fraction in the thin film, hence increasing γ_{LVfilm} locally. Asymmetric γ_{LVfilm} around the droplet causes a net force that drives the droplets towards each other.

To test this mechanism, we next propose a mathematical model to calculate the expected distance L between two identical droplets as a function of time (Fig. 3a, Supplementary Information section 2.4). We start with the diffusion equation to estimate the relative humidity profile around a droplet. By utilizing our prior measurements of θ_{app} of a static droplet as a function of uniform external humidity, we estimate the local γ_{LVfilm} around each droplet as a

3

function of the local relative humidity imposed by the other droplet. Integrating γ_{LVfilm} around the edge we obtain the net force acting on each droplet as $F_{net} = 2\gamma_{LVdrop}mR \int_0^\pi \left(\frac{(1-RH_{room})R\cos(\psi)}{\sqrt{d^2+R^2+2Rd\cos(\psi)}}\right)d\psi$, where m is the slope of the $\cos(\theta_{app})$ vs RH plot (Fig. 2b), R is the radius of the droplet, d is the distance between the droplet centres, and ψ is the parameter of integration. This net force causes droplet motion and is balanced by a viscous drag force (F_{drag}). Here we neglect inertia since the Reynolds number (Re) is smaller than 1 (for typical droplet velocity 1 mm/s and droplet radius 1 mm, $Re \sim 0.3$).

We calibrated F_{drag} by measuring droplet speed on ramps of known angle, observing that it scaled linearly with the velocity (U) as $F_{drag} = C_D \cdot U$ (Extended Data Fig. 6). The drag coefficient C_D was a linear function of the droplet perimeter, consistent with existing theory based on viscous dissipation at three-phase contact lines[29] (Supplementary Information section 2.1 and 2.2, Extended Data Fig. 5 and 6). Equating F_{drag} with F_{net}, we obtain and integrate the instantaneous velocity to arrive at the distance between the two droplets, $L(t)$. Plotting L as a function of $(\tau - t)$ with τ as the time of droplet contact, we observe a good agreement between model and data, with no adjustable parameters (Fig. 3b). In a log-log plot $L(\tau - t)$ behaves as a scaling law of exponent 0.6 at long distance, which is also captured by the model (Fig. 3b inset).

In Fig. 3c, we present a phase diagram of long-range interactions between one pinned droplet and one mobile droplet, as a function of concentration of both droplets. Over a large concentration range the mobile droplet was attracted to the pinned droplet. However, when [PG]pinned >>[PG]mobile, the mobile droplet fled, indicating a repulsive force. We hypothesize that at high PG concentration, the gradient of PG vapour begins to play a role, decreasing γ_{LVfilm} and driving the mobile droplet away.

At short range, two droplets of like concentrations coalesce upon contact. Droplets of sufficiently different concentrations can undergo a prolonged 'chasing phase'[26] as explained by Riegler and Lazar[30] (Fig. 1b). Fluid is directly exchanged between the droplets, as visualized by a fluorescent dye (Supplementary Video 7). This exchange of fluid leads to a surface tension gradient across both the droplets, where the droplet of lower surface tension 'chases' the droplet of higher surface tension, which in turn 'flees' away[30]. Additional subtleties of short-range interactions can be obtained by adjusting concentrations and volumes (Supplementary Information, Extended Data Fig. 7).

Using the fundamental understanding we developed for this system, we built several self-fueled surface tension driven fluidic machines out of the everyday materials such as food colouring, glass slides, and Sharpie™ marker (Supplementary Information section 1.5). First, we used the long-range interactions to create a droplet self-aligner, which aligns randomly placed droplets of identical concentrations in different 'lanes' into a single straight line (Fig. 4a, Supplementary Video 8). Second, we utilized the short-range interactions to create sustained droplet chasing,

during which droplets circled around a single loop for several minutes (Fig. 4b, Supplementary Video 9). We note that since the droplets are unaffected by prior trajectories, the droplets are able to repeatedly cross over their own paths. Third, we created a completely vertical droplet oscillator by placing a large low surface tension droplet beneath a higher surface tension droplet bounded in a lane on a glass slide (Fig. 4c, Supplementary Video10). Finally we created a concentration based autonomous sorter that segregated small droplets into reservoirs based on their surface tension. In this device, we relied on gravity to bring droplets down a ramp, where they sampled wells from low to high surface tension, merging only when they reached a like concentration (Fig. 4d, Supplementary Video 11). These examples illustrate the wide variety of autonomous sensing and motility based devices that can be created using this system

Online Content Methods, along with any additional Extended Data display items and Source Data, are available in the online version of the paper; references unique to these sections appear only in the online paper

References and Notes:

1   Thomson, J. On certain curious motions observable at the surfaces of wine and other alcoholic liquors. *Phil. Mag.* **10**, 330 (1855).
2   Marangoni, C. Über die Ausbreitung der Tropfen einer Flüssigkeit auf der Oberfläche einer anderen. *Annalen der Physik* **219**, 337-354 (1871).
3   Barthlott, W. & Neinhuis, C. Purity of the sacred lotus, or escape from contamination in biological surfaces. *Planta* **202**, 1-8, doi:DOI 10.1007/s004250050096 (1997).
4   Wenzel, R. N. Resistance of solid surfaces to wetting by water. *Ind Eng Chem* **28**, 988-994, doi:Doi 10.1021/Ie50320a024 (1936).
5   Bascom, W. D., Cottington, R. L. & Singleterry, C. R. Dynamic surface phenomena in the spontaneous spreading of oils on solids. (DTIC Document, 1963).
6   Pollack, M. G., Fair, R. B. & Shenderov, A. D. Electrowetting-based actuation of liquid droplets for microfluidic applications. *Appl Phys Lett* **77**, 1725-1726, doi:Doi 10.1063/1.1308534 (2000).
7   Zhang, X., Shi, F., Niu, J., Jiang, Y. G. & Wang, Z. Q. Superhydrophobic surfaces: from structural control to functional application. *J Mater Chem* **18**, 621-633, doi:Doi 10.1039/B711226b (2008).
8   Daniel, S., Chaudhury, M. K. & Chen, J. C. Fast drop movements resulting from the phase change on a gradient surface. *Science* **291**, 633-636, doi:DOI: 10.1126/science.291.5504.633 (2001).
9   Chaudhury, M. K. & Whitesides, G. M. How to make water run uphill. *Science* **256**, 1539-1541, doi:DOI: 10.1126/science.256.5063.1539 (1992).
10   Ichimura, K., Oh, S. K. & Nakagawa, M. Light-driven motion of liquids on a photoresponsive surface. *Science* **288**, 1624-1626, doi:DOI 10.1126/science.288.5471.1624 (2000).
11   Gallardo, B. S. *et al.* Electrochemical principles for active control of liquids on submillimeter scales. *Science* **283**, 57-60, doi:DOI 10.1126/science.283.5398.57 (1999).
12   Brzoska, J. B., Brochard-Wyart, F. & Rondelez, F. Motions of Droplets on Hydrophobic Model Surfaces Induced by Thermal-Gradients. *Langmuir* **9**, 2220-2224, doi:Doi 10.1021/La00032a052 (1993).
13   Style, R. W. *et al.* Patterning droplets with durotaxis. *P Natl Acad Sci USA* **110**, 12541-12544, doi:DOI 10.1073/pnas.1307122110 (2013).
14   Dettre, R. H. & Johnson, R. E. Contact Angle Hysteresis. IV. Contact Angle Measurements on Heterogeneous Surfaces. *J Phys Chem-Us* **69**, 1507-1515, doi:Doi 10.1021/J100889a012 (1965).

15   Saha, S., Golestanian, R. & Ramaswamy, S. Clusters, asters and collective oscillations in chemotactic colloids. *ArXiv e-prints* **1309**, 4947 (2013). <http://adsabs.harvard.edu/abs/2013arXiv1309.4947S>.

16   Theriot, J. A. & Mitchison, T. J. Actin Microfilament Dynamics in Locomoting Cells. *Nature* **352**, 126-131, doi:Doi 10.1038/352126a0 (1991).

17   Berg, H. C. *E. coli in motion*. (Springer, 2004).

18   de Gennes, P.-G., Brochard-Wyart, F. & Quéré, D. *Capillarity and wetting phenomena : drops, bubbles, pearls, waves*. (Springer, 2004).

19   Hoke, B. C. & Patton, E. F. Surface Tensions of Propylene-Glycol Plus Water. *J Chem Eng Data* **37**, 331-333, doi:Doi 10.1021/Je00007a016 (1992).

20   Deegan, R. D. *et al.* Capillary flow as the cause of ring stains from dried liquid drops. *Nature* **389**, 827-829, doi:Doi 10.1038/39827 (1997).

21   Hu, H. & Larson, R. G. Analysis of the effects of Marangoni stresses on the microflow in an evaporating sessile droplet. *Langmuir* **21**, 3972-3980, doi:Doi 10.1021/La0475270 (2005).

22   Truskett, V. & Stebe, K. J. Influence of surfactants on an evaporating drop: Fluorescence images and particle deposition patterns. *Langmuir* **19**, 8271-8279, doi:Doi 10.1021/La030049t (2003).

23   Tanner, L. H. Spreading of Silicone Oil Drops on Horizontal Surfaces. *J Phys D Appl Phys* **12**, 1473-&, doi:Doi 10.1088/0022-3727/12/9/009 (1979).

24   Bernett, M. K. & Zisman, W. A. Prevention of Liquid Spreading or Creeping. *Contact Angle, Wettability and Adhesion, Advances in Chemistry Series* **vol. 43**, 332-340 (1964).

25   Pesach, D. & Marmur, A. Marangoni Effects in the Spreading of Liquid-Mixtures on a Solid. *Langmuir* **3**, 519-524, doi:Doi 10.1021/La00076a013 (1987).

26   Bangham, D. H. & Saweris, Z. The behaviour of liquid drops and adsorbed films at cleavage surfaces of mica. *T Faraday Soc* **34**, 0554-0569, doi:Doi 10.1039/Tf9383400554 (1938).

27   Carles, P. & Cazabat, A. M. Spreading Involving the Marangoni Effect - Some Preliminary-Results. *Colloid Surface* **41**, 97-105, doi:Doi 10.1016/0166-6622(89)80045-9 (1989).

28   Hu, H. & Larson, R. G. Evaporation of a sessile droplet on a substrate. *J Phys Chem B* **106**, 1334-1344, doi:Doi 10.1021/Jp0118322 (2002).

29   Brochard, F. Motions of Droplets on Solid-Surfaces Induced by Chemical or Thermal-Gradients. *Langmuir* **5**, 432-438, doi:Doi 10.1021/La00086a025 (1989).

30   Riegler, H. & Lazar, P. Delayed coalescence Behavior of droplets with completely miscible liquids. *Langmuir* **24**, 6395-6398, doi:Doi 10.1021/La800630w (2008).

Supplementary Information is available in the online version of the paper.

Author Contribution: N.J.C made the original observation. All authors designed the research. N.J.C and A.B. conducted experiments, and all authors interpreted the data; N.J.C. and A.B. developed the models. N.J.C and A.B. wrote the manuscript, and all authors commented on it.
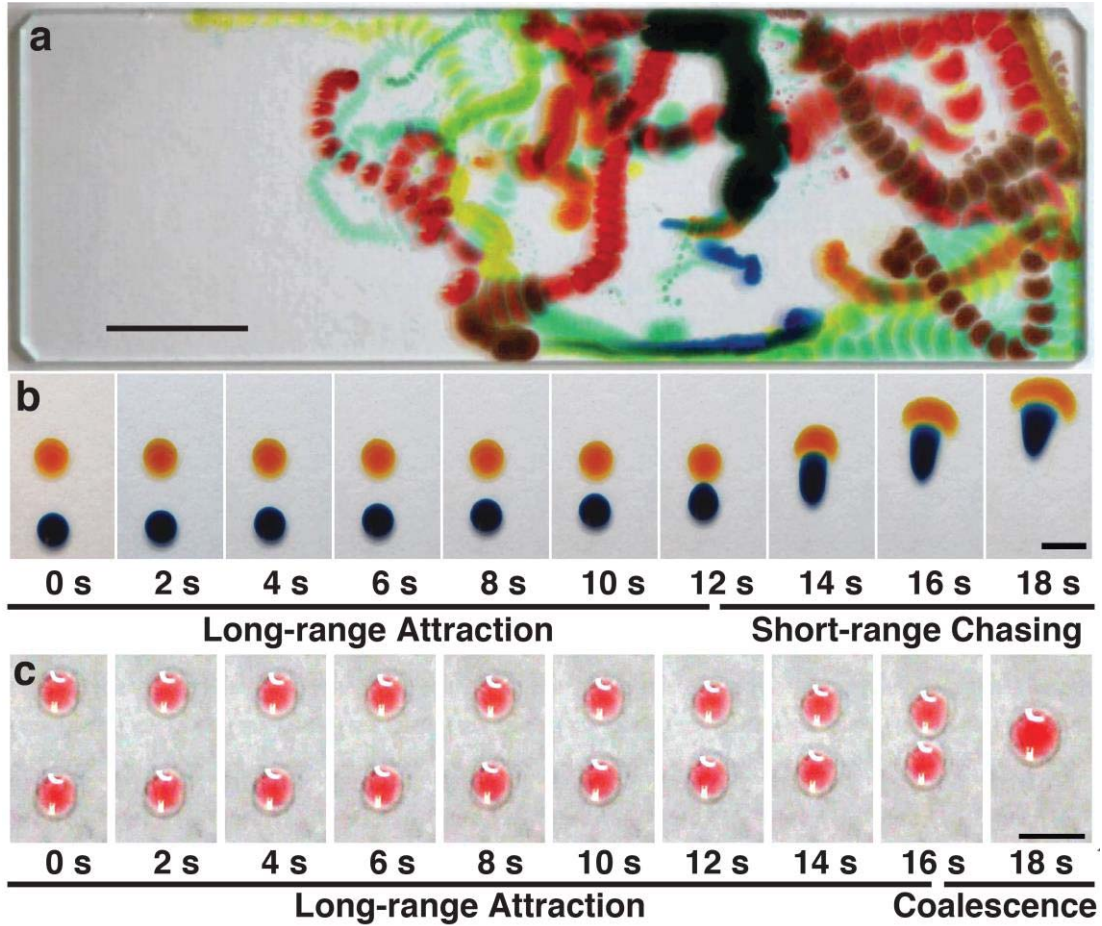
Figures:

Figure 1 | Phenomena. a, Overlaid time lapse of multiple coloured droplets deposited on a clean corona treated glass slide interacting autonomously over 2 minutes. (See Supplementary Video 1, scale bar 10 mm). **b**, Two 0.5 µL droplets of 25% PG (blue) and 1% PG (orange) interacting. The behaviour can be divided into 'long-range attraction' and 'short-range chasing' portions. (See Supplementary Video 2, scale bar 3 mm). **c**, Two droplets of the exact same concentration (0.5 µL 10% PG) also attract each other, through long-range interaction followed by coalescence. All PG % are given as volume percentage in water. (See Supplementary Video 3, scale bar 5 mm).
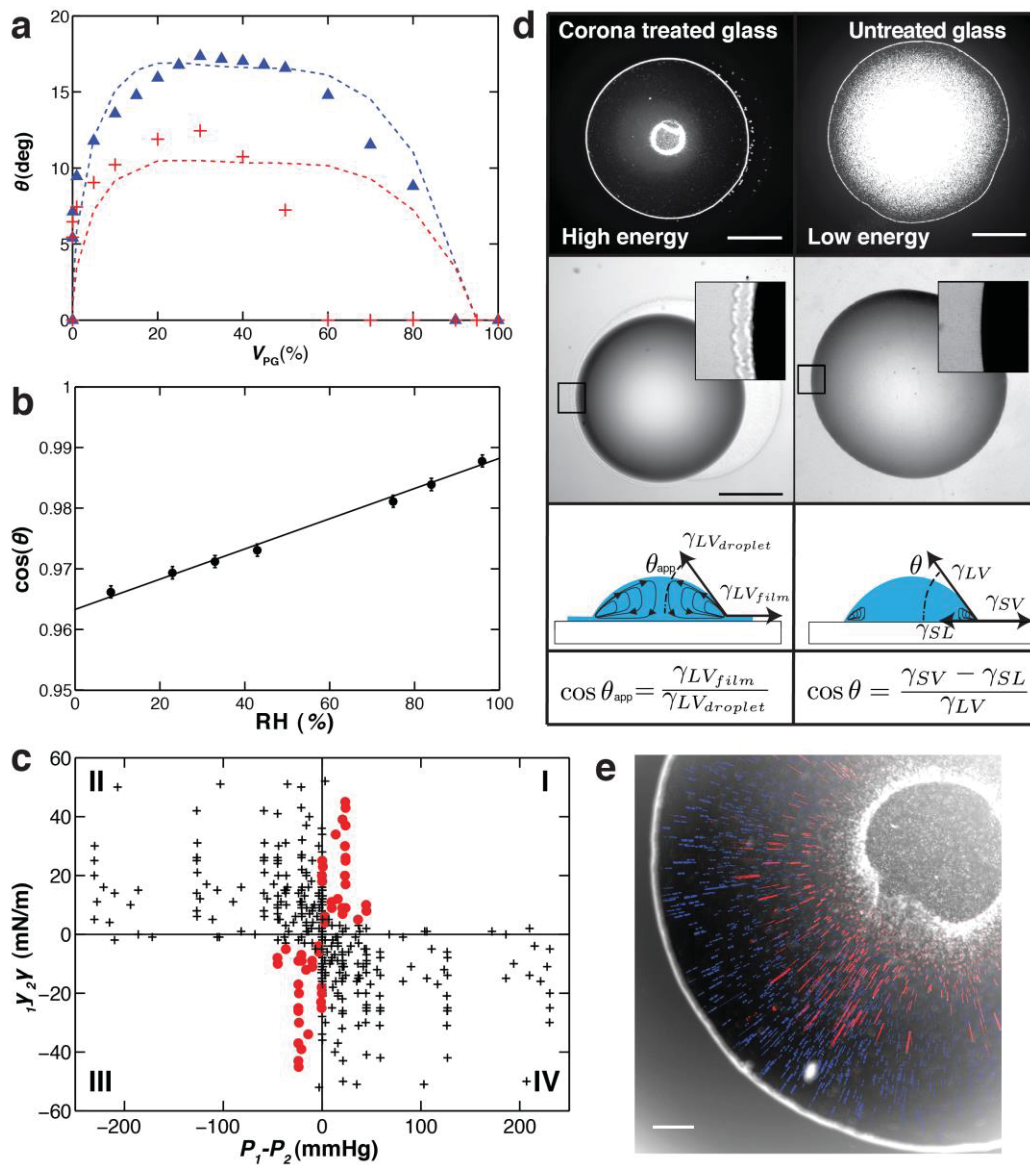
Figure 2 | Individual droplet characteristics. a, Isolated droplets (0.5 μL) on a clean glass surface display a non-monotonic apparent contact angle as a function of PG %. Crosses and triangles indicate data taken at 75% RH and 40% RH respectively. Dashed lines indicate the model's fit to the data. **b**, The cosine of the apparent contact angle varies linearly (line of best fit shown) with external humidity for 0.5 μL 10% PG droplets. Error bars are the range of three measurements at 75% RH. **c**, Behaviour of two-component mixtures of all nonreactive combinations of 21 miscible fluids (see supplementary Table S1 for chemical list) on clean corona treated glass. For each liquid pair, difference in surface tension is plotted against difference in vapour pressure. Red dots indicate droplet formation while black crosses indicate complete wetting. **d**, Important differences between two-component droplets deposited on high and low energy solid substrates. From top to bottom: accumulation of beads at the liquid/vapour

interface, visualization of the thin film (contrast enhanced on insets), flow representation, and force equilibrium, (scale bar 1 mm). **e**, Time lapse trajectories of tracer beads in the droplet. Red traces are focused at the top surface where beads move toward the centre, while blue traces are in the plane close to the glass where beads move outward, (scale bar 200 μm).
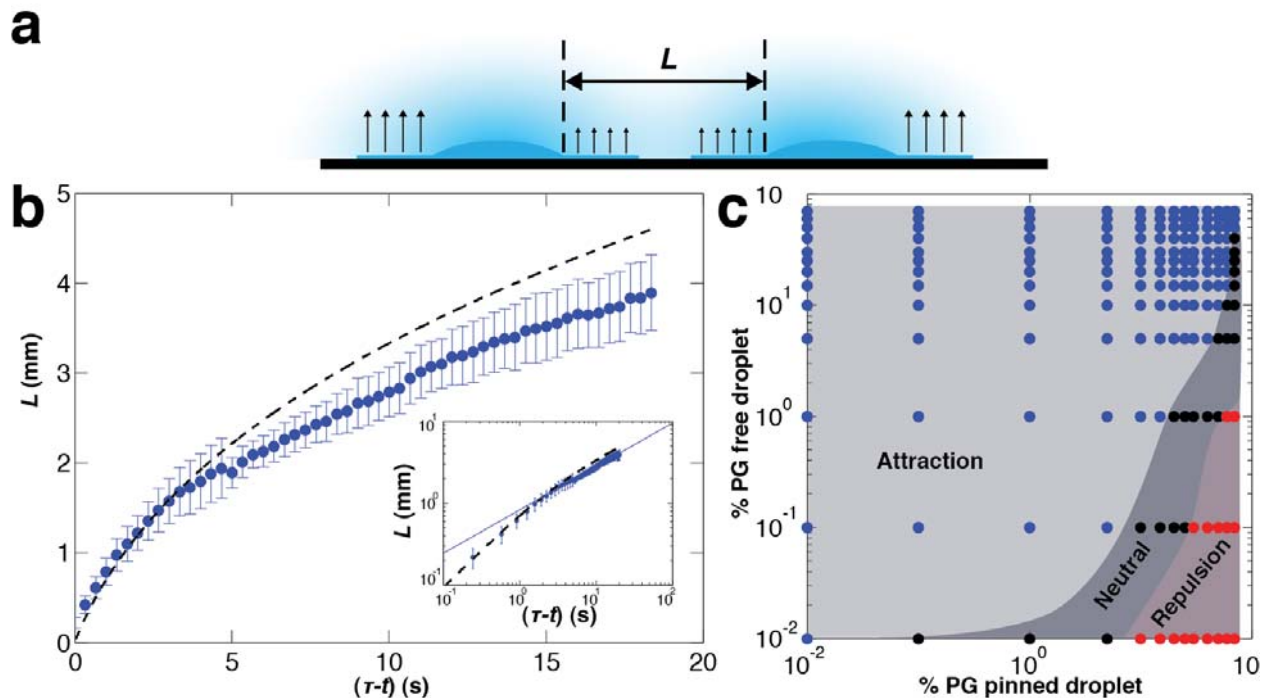

Figure 3 | Long-range droplet interactions. a, Schematic of vapour gradients and evaporation from two droplets distance L apart. Increased vapour concentration between the droplets leads to less evaporation. **b**, Distance between droplets as a function of time before contact for two freely moving 0.5 μL 10% PG droplets. The error bars represent the standard deviation of 12 experiments, and the dashed line is the model prediction, inset: log-log scale, solid line is the power law fit. τ is the time of droplet contact. **c**, Phase diagram of interactions between a single pinned and a single free 0.5 μL droplet (the axes are volume % of PG). Each dot represents an experiment; each colour indicates the direction of motion of the free droplet.
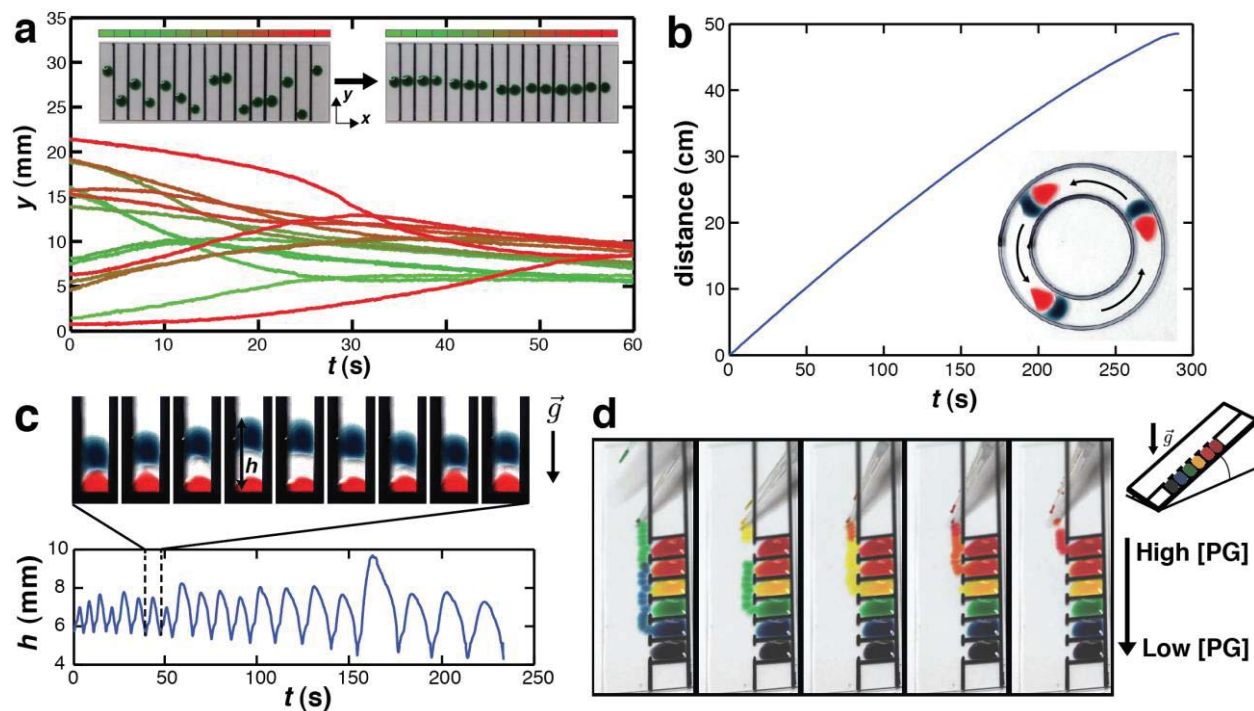
Figure 4 | Droplet based devices. We created four devices by drawing permanent marker (Sharpie™, black) lines, which are hydrophobic enough that droplets do not cross them (Supplementary Videos 8-11). **a**, Spontaneous droplet aligner. Upper left inset: 0.5 μL green droplets of 10% PG are dispensed at random initial positions separated by 5 mm spaced sharpie lines. Upper right inset: droplets have automatically aligned into final positions. The graph shows the y position of each droplet as a function of time. The colour code represents the x position in the aligner. **b**, Short-range chasing between a 1% PG droplet (red) and a 25% PG droplet (blue) in a 2.1 cm mean diameter circle. Inset: a three image time lapse (10 s spacing, arrows representing direction of motion). The graph shows the travelled distance as a function of time. **c**, We deposited a 25% PG droplet (blue) above a 1% PG droplet (red) bounded in a 4 mm lane on a vertical glass slide. The top droplet oscillates up and down. Top: one oscillation, images are separated by 1 s. Bottom: vertical position of the top droplet as a function of time. **d**, Surface tension sorter. Schematic: wells of various concentrations of PG (colours) are confined by sharpie lines (black). Concentrations from top to bottom are 30%, 25%, 20%, 15%, 10%, 5% PG. Each image shows the time lapse trajectory of a droplet as it is deposited at the top and moves down due to gravity, sampling each well, only merging with a well of like concentration. Sorting happens by purely passive means.